

## Fragment Flow and the Multifragmentation Phase Space

G. J. Kunde,<sup>1,\*</sup> W. C. Hsi,<sup>2</sup> W. D. Kunze,<sup>1</sup> A. Schüttauf,<sup>3</sup> A. Wörner,<sup>1</sup> M. Begemann-Blaich,<sup>1</sup> Th. Blaich,<sup>4</sup> D. R. Bowman,<sup>2,†</sup> R. J. Charity,<sup>5</sup> A. Cosmo,<sup>6</sup> A. Ferrero,<sup>7,‡</sup> C. K. Gelbke,<sup>2</sup> J. Hubele,<sup>1</sup> G. Immé,<sup>8</sup> I. Iori,<sup>7</sup> P. Kreutz,<sup>3</sup> V. Lindenstruth,<sup>1</sup> M. A. Lisa,<sup>2</sup> W. G. Lynch,<sup>2</sup> U. Lynen,<sup>1</sup> M. Mang,<sup>3</sup> T. Möhlenkamp,<sup>9</sup> A. Moroni,<sup>7</sup> W. F. J. Müller,<sup>1</sup> M. Neumann,<sup>3</sup> B. Ocker,<sup>3</sup> C. A. Ogilvie,<sup>1,§</sup> G. F. Peaslee,<sup>2</sup> J. Pochodzalla,<sup>1</sup> G. Raciti,<sup>8</sup> T. Rubehn,<sup>1</sup> H. Sann,<sup>1</sup> W. Seidel,<sup>9</sup> V. Serfling,<sup>3</sup> L. G. Sobotka,<sup>5</sup> J. Stroth,<sup>1</sup> L. Stuttge,<sup>6</sup> S. Tomasevic,<sup>6</sup> W. Trautmann,<sup>1</sup> M. B. Tsang,<sup>2</sup> A. Tucholski,<sup>10</sup> G. Verde,<sup>8</sup> C. W. Williams,<sup>2</sup> E. Zude,<sup>1</sup> and B. Zwieglinski<sup>10</sup>

<sup>1</sup>*Gesellschaft für Schwerionenforschung, 64220 Darmstadt, Germany*

<sup>2</sup>*Department of Physics and Astronomy and National Superconducting Cyclotron Laboratory, Michigan State University, East Lansing, Michigan 48824*

<sup>3</sup>*Institut für Kernphysik, Universität Frankfurt, 60486 Frankfurt, Germany*

<sup>4</sup>*Institut für Kernchemie, Universität Mainz, 55099 Mainz, Germany*

<sup>5</sup>*Department of Chemistry, Washington University, St. Louis, Missouri 63130*

<sup>6</sup>*Centre de Recherches Nucléaires, 67037 Strasbourg, France*

<sup>7</sup>*Dipartimento di Fisica, Università di Milano and INFN, 20133 Milano, Italy*

<sup>8</sup>*Dipartimento di Fisica dell' Università and INFN, 95129 Catania, Italy*

<sup>9</sup>*Forschungszentrum Rossendorf, 01314 Dresden, Germany*

<sup>10</sup>*Soltan Institute for Nuclear Studies, 00-681 Warsaw, Hoza 69, Poland*

(Received 9 August 1994; revised manuscript received 6 September 1994)

Fragment distributions have been measured for Au + Au collisions at  $E/A = 100$  and  $1000$  MeV. A high detection efficiency for fragments was obtained by combining the ALADIN spectrometer and the MSU-Miniball/WU-Miniwall array. At both energies the maximum multiplicity of intermediate mass fragments (IMF) normalized to the size of the decaying system is about one IMF per 30 nucleons but the element distributions show significant differences. Within a coalescence picture the suppression of heavy fragments in central collisions at  $E/A = 100$  MeV may be related to a reduction of the density in momentum space which is caused by the collective expansion.

PACS numbers: 25.70.Pq, 24.60.Ky, 25.75.+r

In collisions between two heavy nuclei with beam energies up to about 100 MeV per nucleon the maximum multiplicity of intermediate mass fragments (IMFs) is observed in central collisions [1]. Beyond  $E/A = 100$  MeV a steady decline of the mean fragment multiplicity is seen at small impact parameters [2,3]. The increasing importance of peripheral collisions for the multifragmentation channel at higher energies was revealed by the observation of the “*rise and fall of multifragment emission*” in Au induced reactions at  $E/A = 600$  MeV [4,5].

In peripheral collisions the observed radial motion of fragments with charge  $Z \geq 8$  can be ascribed to the Coulomb repulsion between the produced particles [6], and collective expansion velocities of the decaying spectator nuclei are small. Central collisions in symmetric reactions, on the other hand, exhibit large collective velocities [7–10]. A collective expansion is expected [11–17] to have a strong influence on the fragment formation process. In this Letter we explore the influence of a rapid expansion on fragment formation by comparing the fragment distributions for central Au + Au collisions at  $E/A = 100$  MeV and for peripheral collisions at  $E/A = 1000$  MeV.

The experiments were performed at the SIS heavy ion synchrotron of the GSI facility.  $^{197}\text{Au}$  targets with an areal thickness of 5 and 500 mg/cm<sup>2</sup> were bombarded

with  $^{197}\text{Au}$  ions of  $E/A = 100$  and  $1000$  MeV, respectively. The experiment at  $E/A = 1000$  MeV was performed with the ALADIN forward spectrometer system [18] which allowed efficient detection and identification of projectile fragments with  $Z \geq 2$ . At the lower energy, fragment detection with close to  $4\pi$  coverage was achieved by combining the ALADIN forward spectrometer with the MSU-Miniball/WU-Miniwall array. At polar angles of  $145^\circ \leq \Theta_{\text{lab}} \leq 160^\circ$ , charged particles were detected in 215 plastic-scintillator-CsI(Tl) phoswich detectors of the Miniball [19] and Miniwall. The thin plastic-scintillator foils of the phoswich telescopes allowed identification of the detected fragments by their element number for laboratory energies per nucleon between threshold energies of  $E_{\text{th}}/A \approx 1.5$  MeV (2.5 MeV) and punchthrough energies for the Miniball of  $E_{\text{pu}}/A \approx 80$  (200 MeV) for  $Z = 2$  ( $Z = 10$ ) particles, respectively [20]. Light particles with  $Z = 1$  were isotopically resolved for kinetic energies larger than about 15 MeV and energies per nucleon below 80 MeV [20].

Particles emitted to angles between the Miniball/wall and the ALADIN magnet were detected and separated according to their element number in an 84 element Si-CsI(Tl) hodoscope placed in front of the magnet. Each of these detector elements consisted of a 300  $\mu\text{m}$  thick Si detector and a 6 cm thick CsI(Tl) scintillator.

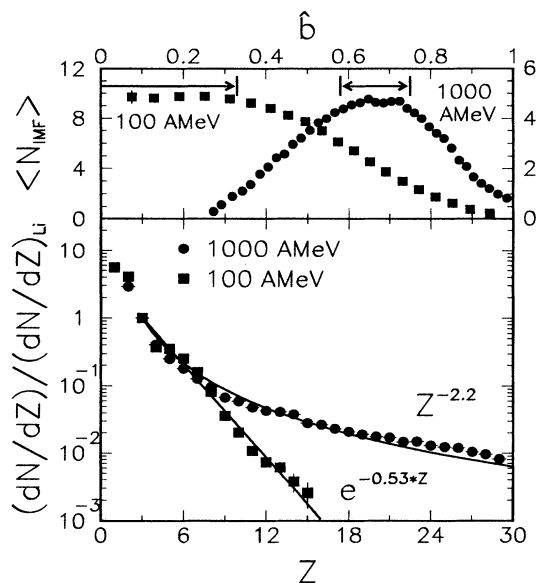


FIG. 1. Top part: Mean multiplicity of detected IMFs with  $3 \leq Z \leq 30$  produced in Au + Au collisions at  $E/A = 100$  MeV (left scale) and 1000 MeV (right scale) as a function of the reconstructed impact parameter  $\hat{b}$ .  $\hat{b} = 1$  corresponds to an impact parameter of about 15 fm. The lower part shows the charge distributions observed in the impact parameter range of maximum mean IMF multiplicity (indicated by the arrows in the upper part of the figure). The lines represent an exponential and power-law fit to the  $Z$  distributions.

The upper part of Fig. 1 shows the mean observed number of IMFs ( $3 \leq Z_{\text{IMF}} \leq 30$ ) as a function of the reduced impact parameter  $\hat{b}$ . The impact parameter scale was derived from the multiplicity of light particles at  $E/A = 100$  MeV [3] and  $Z_{\text{bound}}$  at  $E/A = 1000$  MeV [21]. At  $E/A = 100$  MeV a maximum mean fragment multiplicity of  $\langle N_{\text{IMF}} \rangle \approx 10$  is detected in central collisions [3]. The majority of the fragments originate from the interaction region. At  $E/A = 1000$  MeV, the maximum mean multiplicity of  $\langle N_{\text{IMF}} \rangle \approx 5$  is seen in peripheral collisions. In this case, the projectile spectator is the dominant source of the IMFs. Correcting these numbers for the detection efficiency [22], we find that in both cases the maximum IMF multiplicity normalized to the size of the decaying system is close to one IMF per 30 nucleons. (Adopting a participant-spectator geometry [23], the decaying system is composed of  $2 \times 160$  participating nucleons in central collisions with impact parameters  $b \leq 4.5$  fm at  $E/A = 100$  MeV and of approximately 150 spectator nucleons in peripheral events with  $b \approx 10$  fm at  $E/A = 1000$  MeV.)

The element distribution of fragments produced in collisions corresponding to the maximum mean IMF multiplicity are compared in the lower part of Fig. 1. The selection criteria imposed on the impact parameter are indicated by the arrows in the upper part of Fig. 1. Consis-

tent with previous investigations of Au + Au collisions [2] an exponential charge distribution is observed in central reactions. Although the size of the fragmenting system is smaller at  $E/A = 1000$  MeV, more heavy clusters are produced in peripheral multifragmentation, and the  $Z$  distribution shows a power-law behavior. In the following, we will relate this striking difference to the difference in the collective expansion velocity.

Generally, the fragment momenta  $\vec{p}$  may be decomposed into a random, "thermal" part  $\vec{p}_{\text{thermal}}$ , a collective flow contribution  $\vec{p}_{\text{flow}}$ , and a momentum provided by the Coulomb repulsion  $\vec{p}_{\text{Coulomb}}$ . In the discussion below we assume a random component which is independent of the position  $\vec{r}$  with respect to the center of the decaying system and an ordered velocity which is proportional to  $|\vec{r}|$  [24,25]. In this case, cross terms between the collective and random component vanish on the average, and the total mean kinetic energy  $\langle E \rangle$  may be written as

$$\langle E \rangle = \langle E_{\text{thermal}} \rangle + \langle E_F \rangle, \quad (1)$$

where  $\langle E_F \rangle$  reflects the sum of the initial expansive flow and the Coulomb induced motion [26].

The filled squares in Fig. 2 show the mean kinetic energies per nucleon of fragments at  $E/A = 100$  MeV as a function of the fragment charge for central collisions selected by  $\hat{b} \leq 0.33$  (see Fig. 1). In order to minimize the influence of an additional collective flow along the beam axis caused by noncentral collisions [10,27,28], these data were obtained from fragments emitted to c.m. angles of  $\Theta_{\text{c.m.}} = 90^\circ \pm 10^\circ$ . Subtracting the mean radial flow energies  $\langle E_F/A \rangle$  [29] from the observed mean kinetic energies yields the values for the remaining random kinetic energies per nucleon shown by the open squares in Fig. 2.

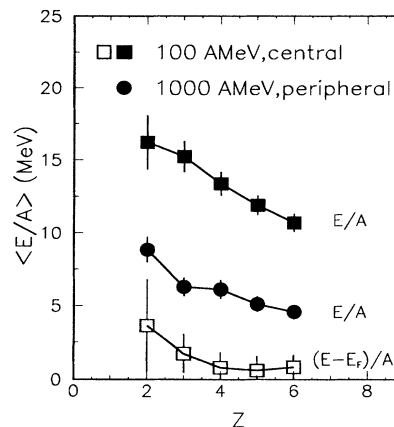


FIG. 2. Mean kinetic energy per nucleon with respect to the center of mass of the decaying system as a function of the fragment charge for peripheral Au + Au collisions at  $E/A = 1000$  MeV (dots) and central reactions at  $E/A = 100$  MeV (squares). The open squares show the difference [29] between the total mean kinetic energy (filled squares) and the flow energy given in Ref. [10].

The dots in Fig. 2 show the average kinetic energies of fragments produced in peripheral collisions at  $E/A = 1000$  MeV. These energies were obtained by converting the widths of the position distributions perpendicular to the bending plane into an energy by assuming an isotropic decay in the projectile frame [5]. Since this procedure neglects any possible collective transverse motion of the decaying projectile fragments, the given values represent upper limits for the mean kinetic energies.

Consistent with a recent analysis of Au induced collisions at about 1 GeV per nucleon [30] mean collective bounce-off momenta observed at  $b \approx 10$  fm vary between approximately 32 MeV/c per particle in Au + Au collisions at  $E/A = 400$  MeV [31] and 25 MeV/c per nucleon in Au + Pb collisions at  $E/A = 600$  MeV [6] and indicate collective transverse energies of 1–2 MeV per nucleon. Coulomb repulsion from a system of 150 nucleons at a density of  $\rho = (0.1-0.5)\rho_0$  will lead to an ordered radial motion in the order of 1.7–3 MeV per nucleon. Subtracting these values from the mean energy gives thermal energies which are compatible with those extracted for  $E/A = 100$  MeV. However, the two systems differ substantially with regard to the magnitude of collective expansion velocities.

A difference in collective velocities will lead to a different mass distribution, e.g., if the fragments are formed by a coalescence mechanism [32]. In order to provide simple analytic relations, we consider a self-similar flow profile superimposed on a spherical, homogeneous, thermally decaying system. For simplicity, the density in momentum space is assumed to be proportional to  $p_{\text{rms}}^{-3}$ , where  $p_{\text{rms}}$  denotes the rms—momentum of the nucleons at freeze-out. The probability that a fragment of mass number  $A$  is formed in collisions which exhibit a flow is then reduced by the factor

$$f_A = [p_{\text{rms}}^{\text{thermal}} / \sqrt{(p_{\text{rms}}^{\text{thermal}})^2 + (p_{\text{rms}}^{\text{flow}})^2}]^{3A} \quad (2)$$

in comparison to a situation without flow but the same freeze-out temperature. The thermal momentum width of the nucleons at freeze-out may be expressed in terms of the breakup temperature  $T$  as

$$p_{\text{rms}}^{\text{thermal}} = \sqrt{3m_0T}, \quad (3)$$

where  $m_0$  denotes the nucleon mass. For a self-similar expansion the flow contribution across the volume which fuses into a fragment is independent of the location of the fragment and is given by

$$p_{\text{rms}}^{\text{flow}} = \sqrt{\langle E/A \rangle_{\text{flow}}} \left( \frac{R_F}{R_S} \right)^2 2m_0. \quad (4)$$

Here,  $\langle E/A \rangle_{\text{flow}}$  is the mean flow energy per nucleon,  $R_S$  is the radius of the source, and  $R_F$  denotes the radius of the spherical coalescence volume of the fragment. For a homogeneous system the ratio  $R_F/R_S$  is given by  $(A_F/A_S)^{1/3}$ , where  $A_S$  stands for the total mass of the system and  $A_F$  is the fragment mass.

In order to compare systems of different mass  $A_S$ , we furthermore apply a correction due to the variation of accessible volume with fragment mass as outlined in Ref. [33] and obtain a total reduction factor

$$f(A_S, \langle E/A \rangle_{\text{flow}}/T) = \frac{[1 - (A_F/A_S)^{1/3}]^3}{[1 + \frac{2}{3}(\langle E/A \rangle_{\text{flow}}/T)(A_F/A_S)^{2/3}]^{3A/2}} \quad (5)$$

which depends only on the total mass of the system,  $A_S$ , and the ratio  $\langle E/A \rangle_{\text{flow}}/T$ .

The observed ratio between the two distributions shown in Fig. 1—normalized at  $Z = 3$ —is given in Fig. 3 by the dots. The lines in Fig. 3 show the ratio

$$\xi(A_F) = \frac{f(A_S = 150, 0)}{f(A_S = 320, \langle E/A \rangle_{\text{flow}}/T)} \quad (6)$$

which compares a system of 150 nucleons having no initial flow (representative for the situation at  $E/A = 1000$  MeV) and a system composed of 320 nucleons with a flow ( $\langle E/A \rangle_{\text{flow}}/T$ ) (representing central Au + Au collisions at  $E/A = 100$  MeV). In order to link the calculations to the observed ratios the curves have been normalized at  $A_F = 6$  and plotted assuming  $A = 2Z$ .

Our schematic coalescence model demonstrates that fragment formation may not only depend on the (local) temperature and density, but that it can be strongly affected by nonuniform collective velocity components. Thus, in the presence of a rapid collective expansion, static statistical models must be modified to incorporate such effects. The calculations indicate that the formation

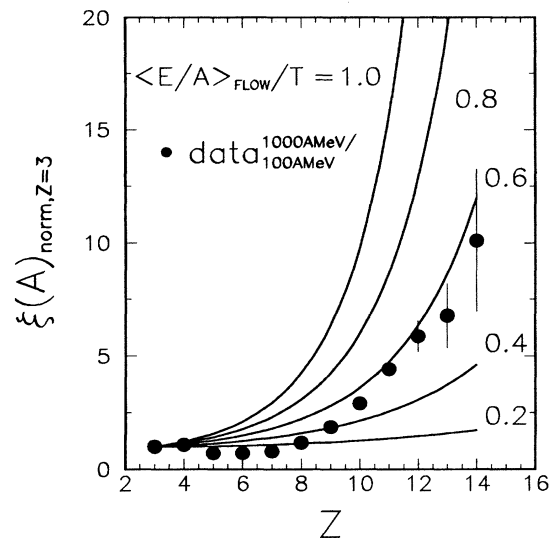


FIG. 3. Suppression of heavy IMFs due to an expansive flow. The dots represent the ratio between the charge distributions measured at  $E/A = 1000$  MeV and 100 MeV (cf. bottom part of Fig. 1). The full lines are results of a simple (analytic) coalescence model which considers the reduction of the density in momentum space due to a radial flow.

probability of heavy fragments is especially sensitive to the underlying flow dynamics. A satisfactory description of the measured intensity ratios of these heavy fragments is obtained for a value  $\langle E/A \rangle_{\text{flow}}/T = 0.5-0.6$ . This ratio is consistent [29] with the results of the flow analysis for light fragments  $Z \leq 6$  reported in Ref. [10].

In summary, increasing the incident energy from 100 to 1000 MeV per nucleon for the symmetric system Au + Au, the peak of the fragment multiplicity was found to shift from central to peripheral collisions. At the same time the source from which the majority of fragments originated changed from the interaction region to the two spectator nuclei. Despite this difference the number of IMFs normalized to the size of the decaying system is nearly the same in both reactions and amounts to about one IMF per 30 nucleons. The element distributions, on the other hand, are significantly different and change from an exponential shape at 100 MeV per nucleon to a power-law behavior at 1000 MeV per nucleon. This dissimilarity could be related to the density in momentum space, which is reduced for central collisions at  $E/A = 100$  MeV because of the high value of expansive flow.

The authors wish to acknowledge the support from the SIS staff. J.P. acknowledges the financial support of the Deutsche Forschungsgemeinschaft under Contract No. Po 256/2-1, and W.G.L. and L.G.S. acknowledge the receipt of U.S. Presidential Young Investigators Awards. This work was supported by the National Science Foundation under Grants No. PHY-90-15255 and No. PHY-92-14992 and the U.S. Department of Energy under Contract No. DE-FG02-87ER-40316.

\*Present address: National Superconducting Cyclotron Laboratory, Michigan State University, East Lansing, MI 48824.

†Present address: Chalk River Laboratories, Chalk River, Ontario K0J 1J0, Canada.

‡On leave from the Comision Nacional Energia Atomica, Argentina.

§Present address: Department of Physics, MIT, Cambridge, MA 02139.

- [1] See, e.g., W. Bauer *et al.*, Nucl. Phys. **A553**, 749c (1993).  
 [2] C. Kuhn *et al.*, Phys. Rev. C **48**, 1232 (1993).  
 [3] M. B. Tsang *et al.*, Phys. Rev. Lett. **71**, 1502 (1993).  
 [4] C. A. Ogilvie *et al.*, Phys. Rev. Lett. **67**, 1214 (1991).  
 [5] J. Hubele *et al.*, Phys. Rev. C **46**, R1577 (1992).  
 [6] V. Lindenstruth, Ph.D. thesis, University Frankfurt, 1993 [GSI Report No. GSI-93-18].  
 [7] H. W. Barz *et al.*, Nucl. Phys. **A531**, 453 (1991).  
 [8] W. Bauer *et al.*, Phys. Rev. C **47**, R1838 (1993).  
 [9] S. C. Jeong *et al.*, Phys. Rev. Lett. **72**, 3468 (1994).  
 [10] W. C. Hsi *et al.*, Report No. MSUCL-930, 1994.  
 [11] D. E. Grady, J. Appl. Phys. **53**, 322 (1982).  
 [12] B. L. Holian and D. E. Grady, Phys. Rev. Lett. **60**, 1355 (1988).  
 [13] J. Desbois, R. Boisgard, C. Ngô, and J. Nemeth, Z. Phys. A **328**, 101 (1987).  
 [14] L. De Paula *et al.*, Phys. Lett. B **258**, 251 (1991).  
 [15] W. A. Friedman, Phys. Rev. Lett. **60**, 2125 (1988).  
 [16] R. Donangelo, A. Romanelli, H. Schulz, and A. C. Sicardi-Schifino, Phys. Rev. C **49**, 3182 (1994).  
 [17] M. Colonna, M. DiToro, and A. Guarnera, LNS report, 1994 (unpublished).  
 [18] ALADIN Collaboration, U. Lynen *et al.*, GSI Report No. GSI-02-89 (unpublished).  
 [19] R. T. DeSouza *et al.*, Nucl. Instrum. Methods Phys. Res., Sect. A **295**, 109 (1990).  
 [20] For the Miniwall-array punchthrough energies are larger by a factor of roughly 1.2.  
 [21] J. Hubele *et al.*, Z. Phys. **340**, 263 (1991).  
 [22] In the region of the maximum mean fragment multiplicity at  $E/A = 1000$  MeV, the detection efficiency for fragments associated with the projectile spectator was  $(97 \pm 2)\%$  and  $(99 \pm 1)\%$  for helium and lithium fragments, respectively, and better than 99% for all heavier fragments. For central Au + Au collisions at  $E/A = 100$  MeV, fragments in the range from  $Z = 2$  to  $Z = 16$  were detected with an Z-independent efficiency of about 80%.  
 [23] J. Gosset, H. H. Gutbrod, W. G. Meyer, A. M. Poskanzer, A. Sandoval, R. Stock, and G. D. Westfall, Phys. Rev. C **16**, 629 (1977).  
 [24] J. P. Bondorf, S. I. A. Garpman, and J. Zimanyi, Nucl. Phys. **A296**, 320 (1978).  
 [25] L. P. Csernai and H. W. Barz, Z. Phys. A **296**, 173 (1980).  
 [26] A collective velocity field proportional to  $|\vec{r}|$  is, for example, caused by a self-similar expansion and also by a Coulomb repulsion when particles are emitted from a spherical volume of uniform density. Without isotopic resolution, the two effects cannot be distinguished (see, e.g., [10]) thus justifying our ansatz in Eq. (1) of a thermal component and a single flow contribution only.  
 [27] H. Stöcker *et al.*, Nucl. Phys. **A387**, 205c (1982).  
 [28] P. Danielewicz and Q. Pan, Phys. Rev. C **46**, 2002 (1992).  
 [29] The flow energies were extracted from fits to the kinetic energy spectra assuming a temperature of  $T = 15$  MeV as described in Ref. [10], whereas the mean kinetic energies were determined for c.m. angles  $\Theta_{\text{c.m.}} = 90^\circ \pm 10^\circ$ . Systematic uncertainties of the flow energy related to changes of the temperature  $T$  between 5 and 20 MeV or to different angular regions, may reach 2 MeV per nucleon (see Ref. [10]). Therefore, the thermal energies shown in Fig. 2 by the open squares have additional systematic uncertainties up to 2 MeV per nucleon.  
 [30] F. P. Brady *et al.*, Phys. Rev. C **50**, R525 (1994).  
 [31] G. J. Kunde, Ph.D. thesis, University Frankfurt, 1994 (unpublished).  
 [32] It should be emphasized though that such a scenario is not the only one which may give rise to a suppression of large clusters. For example, an insufficient time for the cluster formation via nucleation and/or fluctuations [17] due to the rapid expansion may prevent the formation of heavy fragments. A further approach may be based on the balance of the kinetic energy of expansion of a produced fragment on one hand and the potential energy required to create its surface, on the other hand [11].  
 [33] R. Donangelo and H. D. Marta, Phys. Rev. C **46**, 805 (1992).